pISSN 1229-3008 eISSN 2287-6251
Progress in Superconductivity and Cryogenics
Vol.17, No.4, (2015), pp.30~33 http://dx.doi.org/10.9714/psac.2015.17.4.030

Synthesis of the Ni-doped ternary compound $Ba(Fe_{1-x}Ni_x)_2Se_3$

Hyeon Beom Park[a], Soohyeon Shin[a], Soon-Gil Jung[a], Doyeon Hwang[b], Hyoyoung Lee[b], and Tuson Park*[, a]

[a] *Department of Physics, Sungkyunkwan University, Suwon 440-746, Republic of Korea*
[b] *Centre for Integrated Nanostructure Physics (CINAP), Institute of Basic science (IBS), 1Department of Chemistry, 2Department of Energy Science, and 3SAINT, Sungkyunkwan University, 2066 Seoburo, Jangan-gu, Suwon, Gyeonggi-do, 440-746, Republic of Korea*

(Received 14 December 2015; revised or reviewed 25 December 2015; accepted 26 December 2015)

Abstract

We report the synthesis of Ni-doped $BaFe_2Se_3$ single crystals by using a flux method. X-ray diffraction (XRD) of $Ba(Fe_{1-x}Ni_x)_2Se_3$ shows a gradual peak shift with an increase in the nominal Ni-doping rate, x = 0, 0.05, and 0.10, due to a decrease in unit-cell volume. All samples show a spin glass transition, and temperature dependence of magnetic susceptibility shows a negligible change in the spin-glass transition temperature (T_g) with Ni concentration x. The temperature dependence of electrical resistivity for $BaFe_2Se_3$ shows an insulating behavior, and the resistivity value at 295 K and the activation energy (E_a) obtained from the Arrhenius plot decrease with increasing x. These results suggest that the Ni doping can be effectively worked as a dopant for electron charge carriers, but is less efficient in controlling the magnetic property, such as spin glass transition, in the $BaFe_2Se_3$ compound.

Keywords: Ni-doped $BaFe_2Se_3$, Spin glass, Arrhenius plot, Fe-based superconductor

1. INTRODUCTION

Fe-based superconductors have attracted great interest because of a high superconducting transition temperature in spite of including a ferromagnetic element of Fe [1]. Recently, a new Fe-based compound, so called Fe-123, is discovered, which shows not a superconducting but an insulating behavior [2-6]. A possibility of superconductivity in $BaFe_2Se_3$ was suggested by doping or application of pressure because they may decrease the band gap of $BaFe_2Se_3$ [3, 7]. Very recently a pressure-induced superconductivity has been reported in $BaFe_2S_3$ under high pressure of ~ 10 GPa [8, 9]. However, superconductivity in MFe_2Se_3 (M = K, Ba, and Cs) is still not revealed by doping or application of pressure [3, 10].

Considering the suppression of the insulating band gap by Co doping [3], we have focused on the electron doping in $BaFe_2Se_3$. Because Ni has one more electron than Co, Ni substitution into the Fe site may reduce the band gap more effectively than Co doping. In this study, we have synthesized $Ba(Fe_{1-x}Ni_x)_2Se_3$ single crystals, x = 0, 0.05 and 0.10, and their electrical resistivity and magnetic properties are investigated.

2. EXPERMENT

$Ba(Fe_{1-x}Ni_x)_2Se_3$ (x = 0, 0.05, and 0.10) single crystals were fabricated by a Te flux method [2], where Ba piece (99.2%, Alfa Aesar), Fe powder (99.9%, Alfa Aesar), Ni powder (99.9%, Alfa Aesar), Se shot (5N, Alfa Aesar), and Te lump (5N, Alfa Aesar) were used for each element. All elements were inserted into the alumina crucible together with the nominal composition ratio of Ba : Fe : Ni : Se : Te = 1 : 2(1−x) : 2x : 3 : 18 in a glove box under Ar environment, and then the crucible was sealed inside a quartz tube under vacuum ~ 10^{-3} Torr. Next, the quartz ampoule was heated at 800°C for 12 hours, and then temperature was decreased to 550°C with a rate of 5°C/h in a box furnace. Finally, the ampoule was centrifuged at 2,000 rpm. Fig. 1 describes the schematic diagram for the growth process, and the inset shows the picture of fabricated $Ba(Fe_{1-x}Ni_x)_2Se_3$ crystal which is in a needle

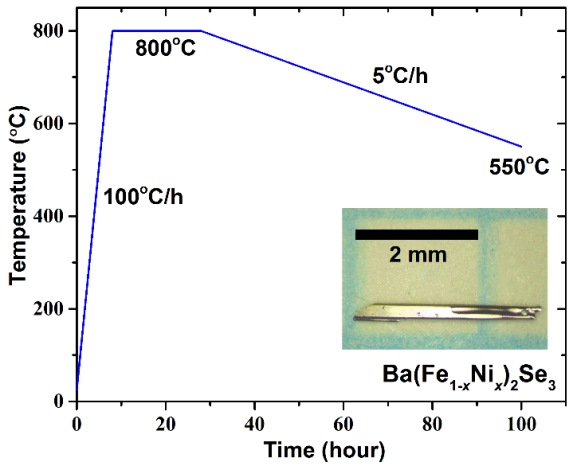

Fig. 1. Temperature profile for the synthesis of $Ba(Fe_{1-x}Ni_x)_2Se_3$ single crystals. Inset shows a fabricated crystal in a needle shape, where the b-axis is the preferred growth direction.

*Corresponding author: tp8701@skku.edu

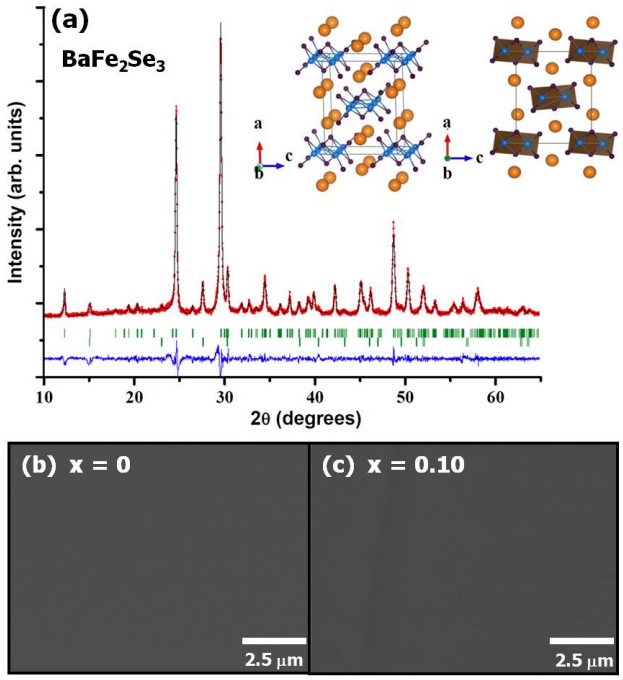

Fig. 2. (a) PXRD patterns of $BaFe_2Se_3$ single crystals. The measured PXRD data is indicated by a red line, and a black line is a fitted line. The blue line is the difference between the red line and black line. The green lines in the upper and lower position are the peak positions of $BaFe_2Se_3$ and Te, respectively. Insets of Fig. 2(a) show the crystal structure of $BaFe_2Se_3$. The orange, blue, and navy balls are Ba, Fe, and Se atoms, respectively. The Fe-Se chains along the *b*-axis are expressed by dark brown color in the right inset. (b) and (c) show the SEM images of surface morphologies for the $BaFe_2Se_3$ and 10% Ni-doped $BaFe_2Se_3$ single crystals, showing the very smooth surface as presented in the inset of Fig. 1.

shape with a typical length of ~3 mm.

The crystal phase and surface morphology were checked by using a powder X-ray diffraction (PXRD, Rigaku) and a scanning electron microscopy (SEM), respectively. Lattice parameters and unit-cell volume were calculated by using a FullProf program. The electrical resistivity was measured by using a closed cycle refrigerator (CCR) with a standard 4-probe method. The magnetic property was investigated by using a magnetic property measurement system (MPMS 5 T, Quantum Design).

3. RESULTS AND DISCUSSION

Figure 2(a) shows powder X-ray diffraction (PXRD) patterns of a $\theta - 2\theta$ scan for the $BaFe_2Se_3$ compound. The inset is the crystal structure of $BaFe_2Se_3$, which is drawn by considering the Wyckoff position mentioned in reference [2]. The χ^2 value is 1.92 in PXRD data, indicating that our analysis is reasonable because the best χ^2 value is close to "1". We calculated lattice parameters and unit-cell volume (*V*) from the PXRD data, and they are $a_0 = 11.7879$ Å , $b_0 = 5.4822$ Å , $c_0 = 9.1815$ Å , and

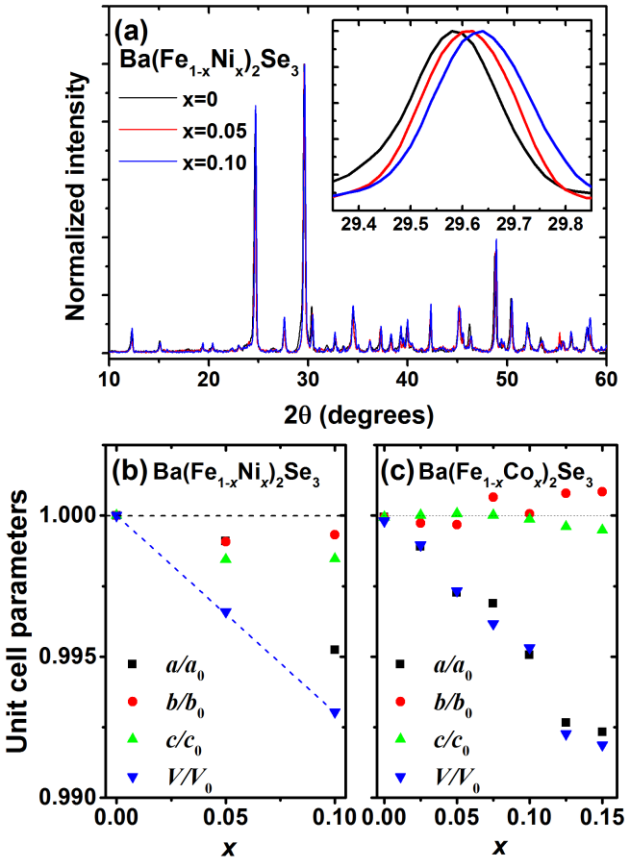

Fig. 3 (a) The PXRD patterns for $Ba(Fe_{1-x}Ni_x)_2Se_3$ with x = 0, 0.05, and 0.10. The intensity is normalized by that at the main peak ($\fallingdotseq 29.6^o$). The systematic peak shift is observed by Ni doping, as shown in inset of Fig. 3(a). (b) and (c) Calculated lattice parameters and unit-cell volume (V) from the PXRD patterns for $Ba(Fe_{1-x}Ni_x)_2Se_3$ and $Ba(Fe_{1-x}Co_x)_2Se_3$, respectively. The data for the $Ba(Fe_{1-x}Co_x)_2Se_3$is adopted from the reference [3] for comparison.

V_0 = 593.329 Å^3. The unit cell consists of a ladder structure along the Fe site to the *b*-axis, as described in the left inset of Fig. 2(a). Fe-Se chains are marked in the right inset of Fig. 2(a). Surface images for the synthesized $Ba(Fe_{1-x}Ni_x)_2Se_3$ single crystals for x = 0 and 0.10 are presented in Figs. 2(b) and (c), respectively, showing the very smooth surface morphologies as presented in the inset of Fig. 1.

The PXRD patterns for the $Ba(Fe_{1-x}Ni_x)_2Se_3$ are presented in Fig. 3(a), and relative changes of lattice parameters and unit-cell volume (V) by a Ni doping are shown in Fig. 3(b). The inset of Fig. 3(a) highlights the PXRD patterns of a $\theta - 2\theta$ scan around main peaks (~29.6^o), where the intensity is normalized by that at the main peak, and a clear peak shift was observed by Ni doping. Lattice parameters and unit-cell volume for the $Ba(Fe_{1-x}Co_x)_2Se_3$ are adopted from the reference [3], as shown in Fig. 3(c), for the comparison with our results. The largest change in lattice parameter was shown along the *a*-axis, which mainly contributes to the change in unit-cell volume (V/V_0). On the other hand, the other lattice parameters along the *b*- and *c*-axis were slightly reduced.

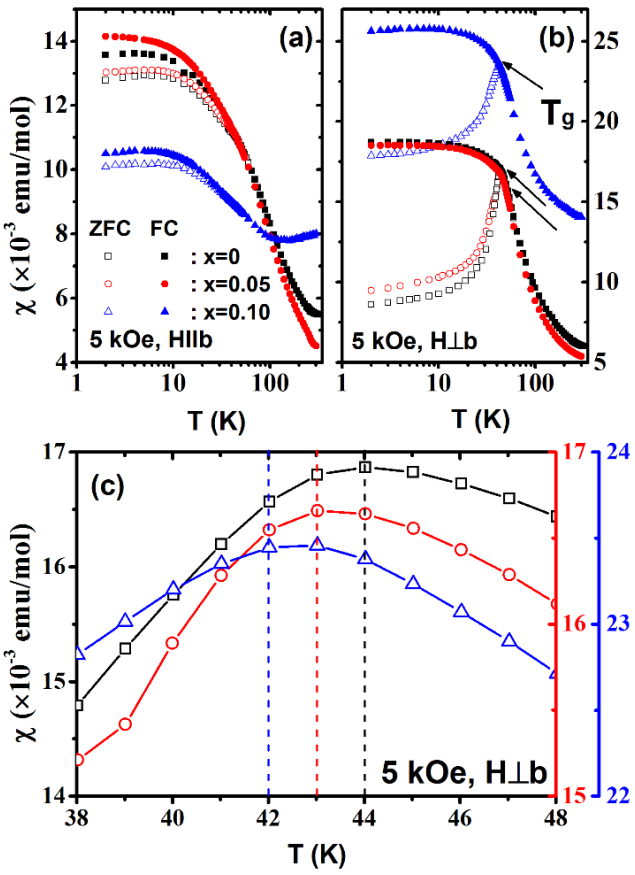

Fig. 4. Zero-field cooled (open symbols) and field cooled (closed symbols) data for $Ba(Fe_{1-x}Ni_x)_2Se_3$ single crystals for (a) *H//b* and (b) *H*⊥*b*, measured at 5 kOe. The irreversible point of ZFC and FC is indicated by arrows in (b), which are related to the spin-glass transition. (c) Enlarged view near the spin-glass transition temperature (T_g). T_g's for Ni concentration x = 0, 0.05, and 0.10, are assigned as the peak in χ in ZFC data. The dashed lines are guides for the eye.

These results are similar to the Co doping, where the lattice parameters *b* and *c* are rarely changed in the $Ba(Fe_{1-x}Co_x)_2Se_3$ [3]. The unit-cell volume is gradually decreased with an increase of the Ni doping rate, as is the case for Co doping.

Figures 4 (a) and (b) show the temperature dependence of magnetic susceptibility (χ) for the $Ba(Fe_{1-x}Ni_x)_2Se_3$ single crystals at 5 kOe applied parallel (*H//b*) and perpendicular (*H*⊥*b*) to *b*-axis, respectively, which were measured by using a magnetic property measurement system (MPMS). A large gap between zero-field-cooled (ZFC) and field-cooled (FC) data for *H*⊥*b* compared to *H//b* indicates that the perpendicular direction to *b*-axis is an easy axis where a spin glass state is formed [3]. The irreversible line between ZFC and FC data, which is marked by arrows in Fig. 4(b), has been ascribed to the spin glass transition in reference [2]. The temperature dependence of χ and the value of χ for x = 0 and 0.05 is very similar, whereas a noticeable change in χ is developed for x = 0.10. This unexpected result appears regardless of the direction of applied magnetic field.

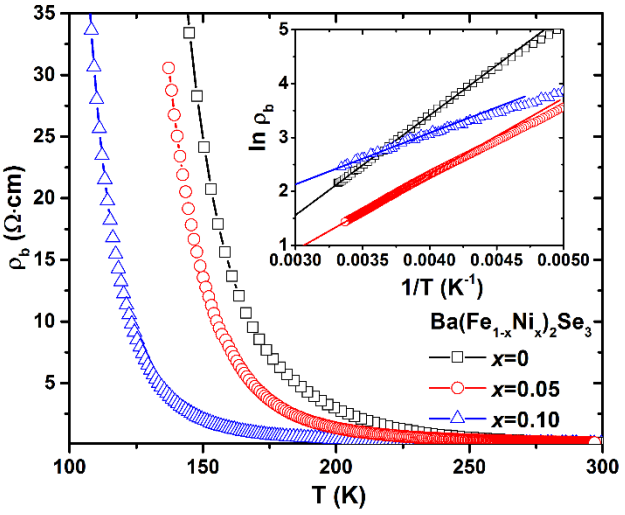

Fig. 5. Temperature dependence of resistivity (ρ_b) for $Ba(Fe_{1-x}Ni_x)_2Se_3$. Inset shows the Arrhenius plot, $\ln\rho \propto \left(\frac{E_a}{2k_B}\right)\left(\frac{1}{T}\right)$, where the activation energy (E_a) corresponds to the band gap and k_B is Boltzmann's constant. The E_a decreases with increasing Ni doping x.

More study is needed to understand the origin of this peculiar behavior at higher Ni concentration. The change in the spin-glass transition temperature (T_g) with the Ni doping rate (x) is shown in Fig. 4(c). The *y*-axis is presented using different colors of black, red, and blue for x = 0, 0.05, and 0.10, respectively. T_g for different Ni concentration, which is assigned as a peak temperature in χ, is marked by the dashed line with different colors. A slight change in T_g indicates that Ni doping hardly affects the magnetic property of $BaFe_2Se_3$. Appearance of spin glass transition in $BaFe_2Se_3$ compounds has been believed to be related to the Fe deficiency arising from different synthesis techniques [2, 5, 6].

Figure 5 shows the temperature dependence of electrical resistivity (ρ_b) of $Ba(Fe_{1-x}Ni_x)_2Se_3$ for electrical current applied along the crystalline *b*-axis. The resistivity at 295 K decreases with increasing Ni doping concentration (x): ρ_b = 0.18, 0.16, and 0.11 Ω·cm for x = 0, 0.05, and 0.10, respectively. These results indicate that Ni doping could provide more electrons to $BaFe_2Se_3$ and reduce the insulating band gap. Reduction in the resistivity is also observed in the Co-doped $BaFe_2Se_3$ because this compound is in proximity to the boundary of metal-insulator transition [3].

Activation energy (E_a) for Ni-doped $BaFe_2Se_3$ compounds was evaluated by using the Arrhenius plot, $\ln(\rho) \propto E_a/2k_BT$. Inset to Fig. 5 shows the least-squares-fit of the logarithmic temperature dependence of the *b*-axis electrical resistivity, where the range of the fitting starts from the highest measured temperature, i.e., 295 K. The activation energy (E_a) obtained from the analysis is 0.320, 0.243, and 0.164 eV for x = 0, 0.05, and 0.10, respectively. Taken together with the decrease in the resistivity at room temperature, the suppression of the activation energy with Ni concentration underscores that Ni substitution for Fe provides additional charge carriers.

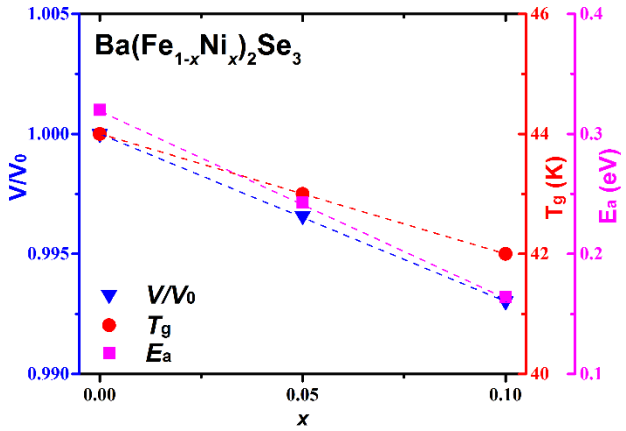

Fig. 6. Ni-doping level (x) dependence of unit-cell volume change (V/V_0), spin glass transition temperature (T_g), and activation energy (E_a). All the characteristic parameters show the same tendency and decrease with increasing x.

Experimental results for the change in unit-cell volume (V/V_0), T_g, and E_a as a function of Ni-doping rate (x) are presented in Fig. 6. The volume change V/V_0 vs x is mainly come from the change in the lattice parameter a, where similar results were also observed in the Co doping case. High pressure up to 8 GPa did not introduce superconductivity in the Co-doped $BaFe_2Se_3$ [3]. In the S-based $BaFe_2S_3$ compound, however, a pressure-induced superconductivity is observed for pressures above 10 GPa, where the largest relative change in the lattice parameter occurs along the b-axis (b/b_0) [8]. The anisotropic compression ratio in this compound indicates that the control of lattice parameter b may be a key parameter to induce superconductivity in the Fe-123 family.

The spin-glass transition temperature (T_g) is not sensitive to the Ni doping, while the activation energy (E_a) is largely suppressed by the Ni doping, as shown in Fig. 6. These results indicate that the Ni doping has more influence on the electrical property than the magnetic property of $BaFe_2Se_3$. In $BaFe_2S_3$, the insulating behavior at ambient pressure is gradually suppressed with increasing pressure and superconductivity is induced near 10 GPa, where electrical resistivity shows a metallic behavior [8, 9]. The correlation between superconductivity and an insulator-metal transition in $BaFe_2S_3$ suggests that the Ni-doped $Ba(Fe_{1-x}Ni_x)_2Se_3$ may become superconducting by applying sufficient pressure or chemical substitution to induce the insulator-metal transition. More work is in progress to confirm this conjecture.

4. CONCLUSION

In conclusions, we have successfully synthesized Ni-doped $BaFe_2Se_3$ single crystals by a Te flux method. Powder X-ray diffraction showed the clear shrinkage of unit-cell volume due to the decrease in the lattice parameter a by the Ni substitution into the Fe site. The spin glass transition was clearly observed in the zero-field cooled and field cooled data for all samples used in this study, $Ba(Fe_{1-x}Ni_x)_2Se_3$ (x = 0, 0.05, and 0.10). The activation energy (E_a) corresponding to the band gap was estimated from the Arrhenius plot, which is remarkably decreased with an increase of Ni doping level (x) in comparison with the spin-glass transition temperature (T_g). We predict that superconductivity may be induced at the critical Ni doping level (x = 0.20), where an insulator-metal transition occurs, i.e., E_a = 0 eV.

ACKNOWLEDGMENT

This work was supported by the National Research Foundation (NRF) of Korea grant funded by the Korean Ministry of Science, ICT and Planning (No. 2012R1A3A2048816).

REFERENCES

[1] Y. Kamihra, T. Watanabe, M. Hirano, and H. Hosono, "Iron-based layered superconductor La[$O_{1-x}F_x$]FeAs (x = 0.05 − 0.12) with T_c = 26 K," *J. Am. Chem. Soc.*, vol. 130, pp. 3296–3297, 2008.

[2] B. Saparov, S. Calder, B. Sipos, H. Cao, S. Chi, D. J. Singh, A. D. Christianson, M. D. Lumsden, and A. S. Sefat, "Spin glass and semiconducting behavior in one-dimensional $BaFe_{2-\delta}Se_3$ ($\delta \approx 0.2$) crystals," *Phys. Rev. B*, vol. 84, pp. 245132, 2011.

[3] F. Du, Y. Hirata, K. Matsubayashi, Y. Uwatoko and Y. Ueda, K, Ohgushi, "Doping- and pressure-induced change of electrical and magnetic properties in the Fe-based spin-ladder compound $BaFe_2Se_3$," *Phys. Rev. B*, vol. 90, pp. 085143, 2014.

[4] F. Du, K. Ohgushi, Y. Nambu, T. Kawakami, M. Avdeev, Y. Hirata, Y. Watanabe, T. J. Sato, and Y. Ueda, "Stripelike magnetism in a mixed-valence insulating state of the Fe-based ladder compound $CsFe_2Se_3$," *Phys. Rev. B*, vol. 85, pp. 214436, 2012.

[5] H. Lei, H. Ryu, A. I. Frenkel, and C. Petrovic, "Anisotropy in $BaFe_2Se_3$ single crystals with double chains of FeSe tetrahedral," *Phys. Rev. B*, vol. 84, pp. 214511, 2011.

[6] Y. Nambu, K. Ohgushi, S. Suzuki, F. Du, M. Avdeev, Y. Uwatoko, K. Munakata, H. Fukazawa, S. Chi, Y. Ueda, and T. J. Sato, "Block magnetism coupled with local distortion in the iron-based spin-ladder compound $BaFe_2Se_3$," *Phys. Rev. B*, vol. 85, pp.064413, 2012.

[7] M. V. Medvedev, I. A. Nekrasov, and M. V. Sadovskii, "Electronic and magnetic structure of a possible iron based superconductor $BaFe_2Se_3$", *JETP Lett.*, vol. 95, pp. 33–37, 2012.

[8] H. Takahashi, A. Sugimoto, Y. Nambu, T. Yamauchi, Y. Hirata, T. Kawakami, M. Avdeev, K. Matsubayashi, F. Du, C. Kawashima, H. Soeda, S. Nakano, Y. Uwatoko, Y. Ueda, T. J. Sato, and K. Ohgushi, "Pressure-induced superconductivity in the iron-based ladder material $BaFe_2S_3$," *Nat. Mater.*, vol. 14, pp. 1008-1012, 2014.

[9] T. Yamauchi, Y. Hirata, Y. Ueda, and K. Ohgushi, "Pressure-induced Mott transition followed by a 24 K superconducting phase in $BaFe_2S_3$," *Phys. Rev. Lett.*, vol. 115, pp. 246402, 2015.

[10] J. M. Caron, J. R. Neilson, D. C. Miller, K. Arpino, A. Llobet, and T. M. McQueen, "Orbital-selective magnetism in the spin-ladder iron selenides $Ba_{1-x}K_xFe_2Se_3$," *Phys. Rev. B*, vol. 85, pp. 180405(R), 2012.